

Euclid & SKA Synergies

Thomas D. Kitching^{*1}, David Bacon², Michael L. Brown³, Philip Bull⁴, Jason D. McEwen¹, Masamune Oguri⁵, Roberto Scaramella⁶, Keitaro Takahashi⁷, Kinwah Wu¹, Daisuke Yamauchi⁸

¹University College London, Department of Space and Climate Physics; ²ICG, University of Portsmouth; ³Department of Physics, University of Manchester; ⁴University of Oslo, Institute for Theoretical Astrophysics; ⁵Graduate School of Science, University of Tokyo, Japan; ⁶INAF-Osservatorio di Roma, I-00040 Monteporzio Catone, Italy; ⁷Graduate School of Science and Technology, Kumamoto University, Japan; ⁸Research Center for the Early Universe, University of Tokyo, Japan;
E-mail: t.kitching@ucl.ac.uk

Over the past few years two of the largest and highest fidelity experiments conceived have been approved for construction: Euclid is an ESA M-Class mission that will map three-quarters of the extra galactic sky with Hubble Space Telescope resolution optical and NIR imaging, and NIR spectroscopy, its scientific aims (amongst others) are to create a map of the dark Universe and to determine the nature of dark energy. The Square Kilometre Array (SKA) has similar scientific aims (and others) using radio wavelength observations. The two experiments are synergistic in several respects, both through the scientific objectives and through the control of systematic effects. SKA Phase-1 and Euclid will be commissioned on similar timescales offering an exciting opportunity to exploit synergies between these facilities.

Advancing Astrophysics with the Square Kilometre Array
June 8-13, 2014
Giardini Naxos, Italy

*Speaker.

1. Introduction

In this Chapter we will describe the ESA Euclid mission, and discuss some of the synergies that Euclid has with the SKA. Euclid probes the low redshift Universe, through both weak lensing and galaxy clustering measurements. The SKA has the potential to probe a higher redshift regime and a different range in scales of the matter power spectrum, linear scales rather than the quasi-non-linear scales that Euclid will be sensitive to, that will make the combination particularly sensitive to signatures of modified gravity and neutrino mass. In combination a longer baseline in redshift will improve expansion history and growth of structure measurements leading to improved measurements of the redshift behaviour of the dark energy equation of state. The cross correlation between Euclid and SKA weak lensing (shape as well as size and flux magnification), Euclid and SKA galaxy clustering (BAO and redshift space distortions), SKA 21cm intensity mapping and Planck data (CMB, SZ and ISW) will provide a multitude of cross-correlation statistics.

As an example of the benefit of combining the experiments for systematic control for the primary science, the shape measurement from Euclid and SKA will be affected by systematics in different ways, meaning that a cross-correlation of the weak lensing data from both data sets will be less prone to shape measurement biases (see Brown et al., in this volume). Furthermore the intrinsic (un-lensed) ellipticity alignments measured by both Euclid and the SKA will have mutual benefit. Specifically, in addition to Euclid, for weak lensing SKA contributes i) depth, providing more source counts for weak lensing, ii) a way to cross-calibrate shape systematics, iii) a way to cross-calibrate intrinsic alignments, and iv) precise redshifts through 21cm line observations. And possibly the use of polarisation and 21cm rotational velocities for intrinsic shapes and lensing tomography of high redshift 21cm fluctuations.

In addition to the primary science objectives of Euclid there is a plethora of additional legacy and cosmology synergies. We can expect $> 10^5$ strong lens detections from Euclid and SKA, many with redshifts for the lenses and sources and high-resolution images. The combination of Euclid and SKA will better investigate the obscured cosmic star formation history as a function of redshift and environment thanks to their combination of areal coverage and sensitivity. For population III, hypernovae and Type II supernovae NIR emission will be detectable by Euclid from supermassive Pop III supernovae in dense 10^7 - $10^8 M_{\odot}$ haloes out to $z = 10 - 15$, and radio synchrotron emission from Pop III supernova remnants detectable by SKA out to $z = 20$.

A further synergistic aspect is that each of these areas will require post-operation infrastructure development in terms of a very large number of hydrodynamical and N-body simulations to understand the effects of non-linear clustering and baryonic feedback. Finally the data analysis of giga-scale catalogues, peta-bytes of data, and post-operation simulations require astrostatistical and astroinformatics synergies for astronomers to access and visualise these data sets.

1.1 Euclid Overview

Euclid¹ is one of the European Space Agency's (ESA) medium (M) class missions that has been selected as part of ESAs "cosmic visions" programme. Euclid was selected by ESA in October 2012, to take the second of the M-class mission places, M2, which means that there is a scheduled

¹<http://euclid-ec.org>

launch date for 2020. The science objective of Euclid is primarily to determine the nature of the the phenomenon that is causing the expansion rate of the Universe to accelerate; so-called ‘dark energy’. However the top-level science objectives are in fact four-fold and cover all current major open questions in cosmology:

- Dynamical Dark Energy: Is the dark energy simply a cosmological constant, or is it a field that evolves dynamically with the expansion of the Universe?
- Modification of Gravity: Alternatively, is the apparent acceleration instead a manifestation of a breakdown of General Relativity on the largest scales, or a failure of the cosmological assumptions of homogeneity and isotropy?
- Dark Matter: What is dark matter? What is the absolute neutrino mass scale and what is the number of relativistic species in the Universe?
- Initial Conditions: What is the power spectrum of primordial density fluctuations, which seeded large-scale structure, and are they described by a Gaussian probability distribution?

More quantitatively the objective of Euclid is to achieve a dark energy Figure of Merit (Albrecht et al. 2006) of ≥ 400 and to determine the growth index γ , that provides a simple parameterisation for deviations from general relativity, to an accuracy of 0.02. Euclid is designed to achieve these science objectives with support from ground-based observations. In combination with the SKA it is expected that the combined strength of these experiments will enable both to far exceed their singular goals. In order to achieve these science objectives Euclid will use two primary cosmological probes: weak lensing and galaxy clustering. These are given equal priority in the mission and indeed it is only through the combination of weak lensing and galaxy clustering that the science objectives can be achieved. In addition Euclid will provide the astronomy community with a rich data set that will enable many astrophysical studies; areas in Euclid that are referred to as ‘Legacy’ science.

The SKA science goals are synergistic with those of Euclid. Whilst Euclid is a focussed experiment to address a particular goal, the SKA design allows for flexibility in the type of science questions that can be addressed. In this case proposals for SKA observations can be tailored to be in the best synergy with Euclid. The Euclid mission has been designed given particular constraints on the telescope size and overall cost of the mission and instrumentation. An optimisation during the Euclid Assessment Phase (Laureijs 2009) that was refined and elaborated during the Definition Phase (Laureijs et al. 2011) of the mission. This resulted in a nominal design of Euclid being a 1.2 meter Korsch, 3 mirror anasigmat telescope. There will be two instruments on board: the VISible focal plane instrument (VIS) (Cropper et al. 2012) and the Near Infrared SpectroPhotometric (NISIP) instrument.

VIS will provide high-resolution optical imaging over a field of view of size 0.787×0.709 square degrees, with a resolution of 0.18 arcseconds, over a single broad-band wavelength range of 550-900 nm (an optical band equivalent to an RIZ filter, although Euclid in fact does not have an optical filter on board). It will consist of 36 4k×4k CCDs. The primary purpose of the VIS instrument is to provide imaging to enable the measurement of galaxy ellipticities to sufficient

accuracy and precision for use in weak lensing. It will image approximately 1.5 billion galaxies with a limiting R-band magnitude of 24.5 (10σ extended source).

NISP has a field of view of a similar size to VIS of 0.763×0.722 square degrees, these are matched to enable simultaneous/matched observations of the sky. The focal plane will contain 16 $2k \times 2k$ HgCdTe (“Mer-Ca-Tel”) detectors. There will be 3 NIR filters, that will enable imaging, and 2 grism spectroscopic elements, that will enable slitless spectroscopy (with an approximate resolution of $R = 250$). The imaging is designed to enable photometric measurements of the same galaxies observed using the VIS instrument for the determination of photometric redshifts for weak lensing. The spectroscopy is designed to enable precision redshifts to be determined for galaxy clustering measurements.

In order to achieve the photometric redshift required for the weak lensing science Euclid will use ground-based optical imaging data from DES and KiDS, and any other available surveys; requiring normal broad-band imaging over the VIS wavelength range. Spectroscopic redshifts from ground-based surveys such as BOSS, DESI and MOONS will also be ingested and used for photometric redshift calibrations.

Every aspect of Euclid is designed using a systems engineering approach where the science requirements are translated into progressively more detailed requirements on survey, telescope and instrument design, as well as requirements on the algorithms used in the data processing. This flow of requirements is described in a series of ESA documents (for example the Euclid SciRD) and related publications (for example (Cropper et al. 2013)). With regard to instrument designs, Euclid and the SKA are therefore synergistic in the sense that Euclid will observe in the optical and NIR wavelengths and SKA will observe at longer radio wavelengths. As we will discuss in this article this enables unique scientific synergies to be exploited when combining the data between the two experiments.

1.2 Survey Synergies

The Euclid primary probes, weak lensing and galaxy clustering, will be carried out over the same area of sky in a wide-field survey of 15,000 square degrees. As described in Laureijs et al. (2011) the area is driven by an optimisation between the galaxy clustering (that prefers a wider area for a fixed observing time) and weak lensing (that can prefer a shallower deeper survey for intrinsic alignment mitigation), as well as efficiency in survey design whereby the lowest 30 degrees in ecliptic latitude are not observed to avoid zodiacal light contamination. In Figure 1 we show the Euclid reference survey from Amiaux et al. (2012) and how this builds as a function of time. It is self-evident that the areal coverage of Euclid and SKA is synergistic with both experiments expected to observe significant fractions of the extragalactic sky. The synergy of the Euclid and SKA experiments in time is also self-evident. Euclid is a nominally 6 year mission that is scheduled to begin observations in 2020, SKA is scheduled to begin construction in 2018 and begin observations on a similar time scale to Euclid.

The depth of the Euclid and SKA surveys is also synergistic, Euclid will have a limiting magnitude in optical wavelengths that will mean it is sensitive to galaxies with redshifts over the range $0 < z < 2$, and the NIR spectroscopy will be sensitive to galaxies at slightly higher redshifts. In Figure 2 we show as an example the normalised distribution of weak lensing galaxies that the SKA phase 1 and the full SKA, over 3π steradians, and the Euclid weak lensing survey will cover.

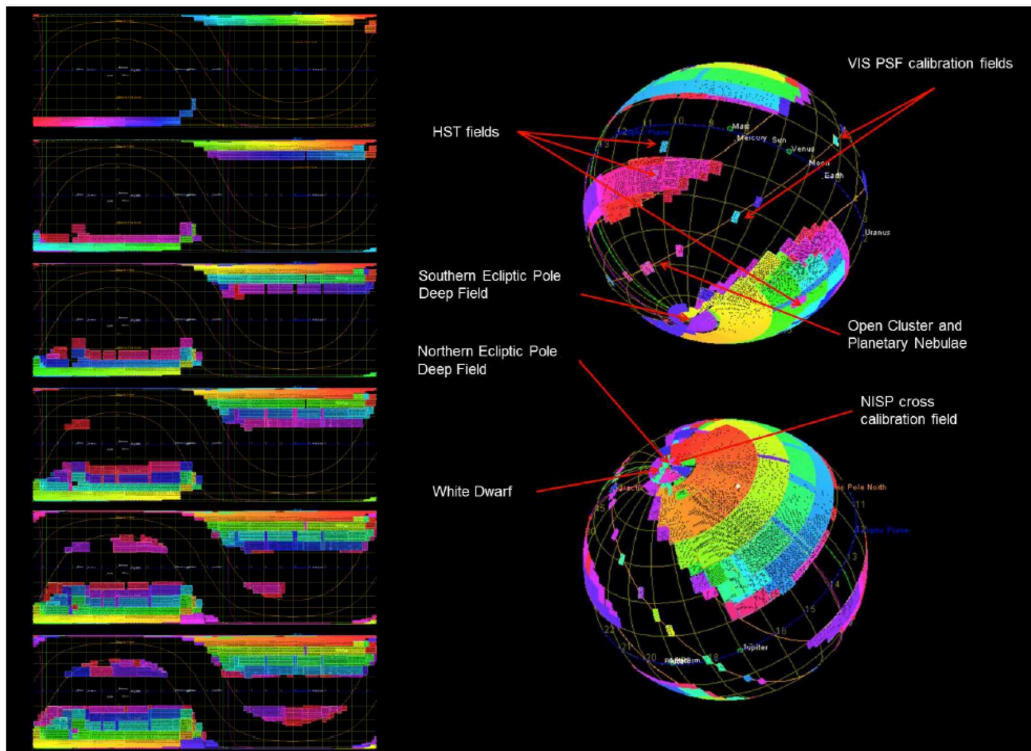


Figure 1: From Amiaux et al. (2012). Euclid Reference Survey construction from year 1 (top) to year 6 (bottom) in cylindrical (left) and orthographic projection. In the left panel, only the wide survey fields are shown. In the right panel, the calibration fields are also displayed.

The Euclid weak lensing survey will have 30 galaxies per square arcminute with size larger than 1.5 times the PSF (R^2) and magnitude $RIZ \leq 24.5$. The SKA survey area and number density has several possibilities, with various area and redshift overlap scenarios (see continuum survey overview, also Brown et al. and Jarvis et al. in this volume), for example for the full SKA (or SKA phase 2) there could be either

- 3π steradian survey: RMS noise = 0.5 micro-Jy, 10 gals arcmin $^{-2}$.
- 5000 sq. deg survey: RMS noise = 0.2 micro-Jy, 23 galaxies arcmin $^{-2}$.
- 1000 sq. deg survey: RMS noise = 0.1 micro-Jy, 37 galaxies arcmin $^{-2}$.

In the remainder of this article we will discuss the scientific synergies that instrument and survey designs of Euclid and the SKA enable.

2. Cosmological Synergies

The primary objectives of Euclid are cosmological in nature, in synergy with SKA these objectives can be supplemented and extended. Both the SKA and Euclid will be able to measure:

- Weak lensing shear g ,

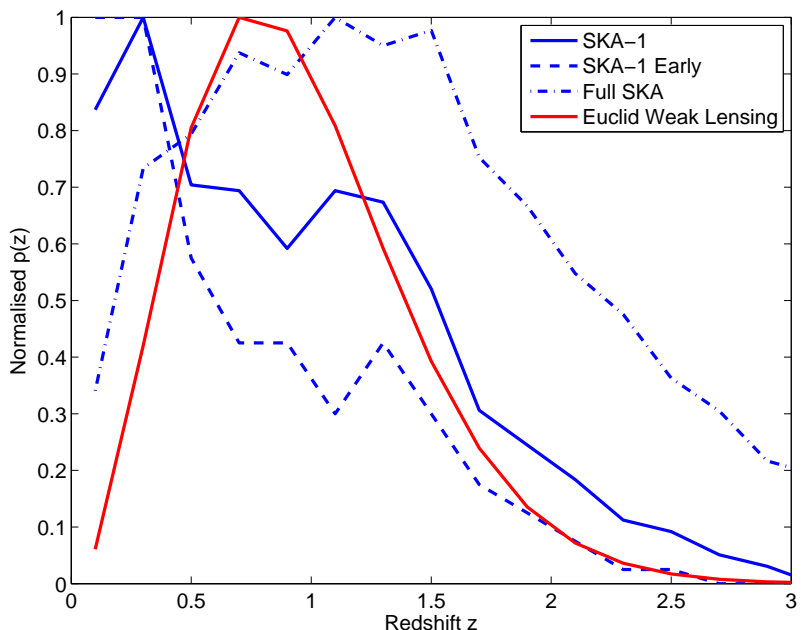


Figure 2: The normalised distributions of galaxies usable for weak lensing analyses in Euclid and the SKA, for the different phases. The numbers for SKA are derived from specifications quoted in the SKA Imaging Science Performance memo which is in turn based on the SKA-1 Baseline Design and from the SKADS simulations of Wilman et al. (2008). The instrument of choice is SKA-MID and it has been assumed Band 2 (950-1760 MHz) has been used which, under the current version of the SKA-1 baseline design gives the best performance in terms of sensitivity at the required angular resolution.

- Weak lensing magnification; including size s and flux ($n(z)$),
- Galaxy positions, both photometric θ_p , and spectroscopic θ_s .

This results in 10 2-point observables, power spectra, in total that can be combined combinatorially to produce 55 cross and auto-correlation statistics. If, for example, a ‘tomographic’ approach is pursued and the galaxy populations are split into > 10 redshift bins then this results in over 5000 power spectra that could be computed including all inter and intra-bin correlations. Some of these correlations can be used to reduced systematic effects, for example the correlation of galaxy shear with galaxy position can be used in infer the intrinsic alignment systematic in cosmic shear studies, see for example Joachimi et al. (2011), or the correlation between weak lensing shear in the radio and optical data sets can be used to reduce ellipticity measurement systematics. Some of these correlations can be used to increase the statistical precision of the combined data, for example the combination of weak lensing shear and size (Heavens et al. 2013). The SKA can also measure unresolved 21cm intensity to create maps that can then be included as an additional cosmological probe to be included in the synergistic combination of probes.

We will highlight just a few of these combinations as examples in this chapter.

2.1 21 cm Intensity Mapping

The principal advantage of 21cm intensity mapping (IM; see Santos et al., in this volume) over

traditional galaxy redshift surveys is that extremely large volumes can be surveyed in a relatively short time; for example, Phase I of the SKA will be capable of surveying a total area of $\sim 30,000$ deg² from $z = 0$ to 3 over the course of 1-2 years. This ability stems from the modest resolution requirements of the IM method; there is no need to resolve individual galaxies, and only the integrated HI emission on comparatively large angular scales matters. We refer to the Chapters on Intensity Mapping and RSD with SKA for more details of this science synergy.

At its most basic, a large IM survey with a Phase I SKA array would complement Euclid simply by increasing the total volume being probed. Consider a situation in which Euclid and the SKA targeted independent survey volumes. The sensitivity of SKA-IM to the first BAO acoustic peak would be comparable to that of Euclid, which is practically cosmic variance-limited at these scales anyway; doubling the survey volume would therefore have a significant effect in beating down cosmic variance and increasing the precision of BAO distance indicators and other observables.

Preventing the surveys from overlapping would spoil a number of interesting opportunities, however. Probing the same volume with two almost cosmic variance-limited experiments is not redundant; as well as providing useful cross-checks for consistency between the two, one can also benefit from the ‘multi-tracer’ effect (see Section 2.3), whereby one can continue to gain information about some observables in spite of cosmic variance as long as different populations of tracers can be distinguished by each survey. This can be used to enhance the precision of redshift space distortion measurements, for example, which probe the growth of structure.

SKA IM surveys are capable of significantly extending the redshift range of Euclid, which covers $0 < z < 2$. By ‘filling in’ redshifts missed by the galaxy survey, one can gain a great deal of leverage on key cosmological functions such as the equation of state of dark energy and the linear growth rate; and could also be used for cross-correlations to get better photometric redshifts for Euclid. Figure 3 shows the joint constraints that can be achieved on w_0 and the growth index, γ , through the combination of Euclid and an SKA-IM survey with much wider redshift coverage. The additional information at low redshift helps to pin down the evolution of dark energy and possible deviations from the standard growth history, while constraints at higher redshift act as a useful ‘anchor’, by locating the transition from the matter-dominated era and putting limits on the spatial curvature, Ω_K .

2.2 Neutrino Physics

Measuring neutrino properties is potentially a particularly interesting area of Euclid-SKA science. Massive neutrino suppress the growth of structure via free-streaming effects introducing an effective pressure that acts in regions of higher density. This continues until the neutrinos become non-relativistic. This transition imprints a feature at a particular scale in the matter power spectrum. As shown in Jimenez et al. (2010) an all-sky Euclid-like survey combined with a galaxy clustering survey, such as that could be achieved by the final SKA, may even be able to determine the neutrino hierarchy.

2.3 Multi-Tracer Method

The SKA and Euclid will observe a huge number of galaxies, and the errors in power spectrum of galaxies will be dominated by cosmic variance, rather than shot noise, at cosmological scales.

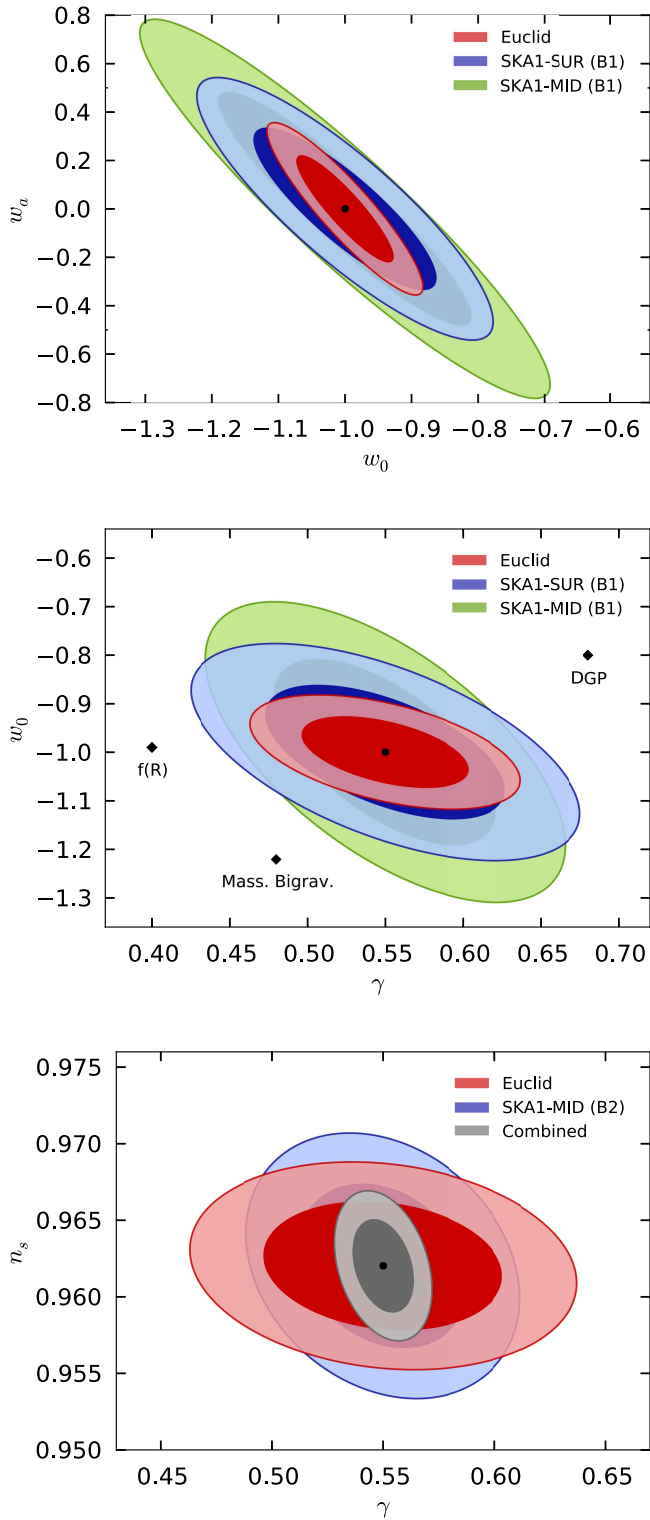


Figure 3: Predicted 1σ, 2 parameter, error contours for dark energy (w_0 , w_a), modified gravity (γ), and initial condition (n_s) parameters for Euclid galaxy clustering and SKA phase 1 design.

This is especially serious when we try to constrain primordial non-Gaussianity whose effect is stronger at larger scales. Cosmic variance could be avoided with a the ‘multi-tracer’ method Seljak (2009) which uses multiple tracers of the dark matter distribution with different biases to cancel out sample variance. Although power spectra of tracers themselves are limited by cosmic variance, the ratio of the power spectra of two tracers, which represents the relative bias, can evade cosmic variance and is limited only by shot noise. Because the mass and redshift dependences of bias are affected by non-Gaussianity (f_{NL}), it can be constrained by the measurements of relative biases.

This multi-tracer method is effective when the bias difference, hence mass difference, is large between tracers and it is critically important to estimate the mass of the dark matter halo hosting each galaxy. A deep survey is also important because bias evolves rapidly with redshift. The SKA and Euclid surveys will have different redshift-distributions of observed galaxies so that their combination enhances the power of multi-tracer method. Yamauchi et al. (2014) studied the potential of combination of the SKA continuum survey and Euclid photometric survey for the constraint on f_{NL} . The SKA continuum survey reaches much further than the Euclid photometric survey, providing a larger redshift range in combination, while the number of galaxies observed by Euclid is larger than that by the SKA at low redshifts, so they are complementary to probe the evolution of bias. Figure 4 shows expected constraints on f_{NL} from Euclid, SKA phase 1, the full SKA and their combinations. Here, it is assumed that galaxies observed by Euclid have photometric redshifts while SKA cannot obtain redshift information (this is a very conservative assumption, but see (Camera et al. 2014) for gains made by using optical and near IR photometric redshifts). It is seen that the constraint on f_{NL} can reach below unity and approach $O(0.3)$.

2.4 Magnetic Fields

The two pressing questions regarding cosmic magnetism are: what is the origin of the cosmological magnetic fields and how do these magnetic fields affect (or were affected by) the structure formation and evolution of the Universe? In a more practical perspective, we would like to know how the cosmological magnetic fields imprint observational signatures and how we can make use of these signatures to better understand the structural formation process in our Universe.

Charged particles in the presence of a magnetic field experience a Lorentz force. As such the presence of a primordial magnetic field would produce and amplify density fluctuations in ionised gas (the baryons). Through gravitational coupling between the baryons and the dark matter, the magnetic field would imprint signatures in the dark matter density distributions. As magnetic fields alter the matter density power spectrum and the halo mass function, the magnification bias and the redshift distribution of galaxies are distorted (see Fedeli & Moscardini (2012); Camera et al. (2014)). The capability of Euclid weak lensing studies (and SKA weak lensing studies) together with the Faraday rotation measurements using the SKA will be able to quantify such a mechanism, which will not only set constraints on the strength of the magnetic fields in the early Universe but also determines the role of magnetic interaction in cosmological structure formation, which has been assumed to be solely gravitational.

Gravitational lensing, both weak and strong, are powerful tools in the studies of cosmological large-scale structures. Lensing calculations rely on ray tracing in a geometrical framework set using the theory of relativity, however absorption and scattering of photons emitted from the distant lensed sources along the ray are usually ignored. This may well be a sensible first approximation,

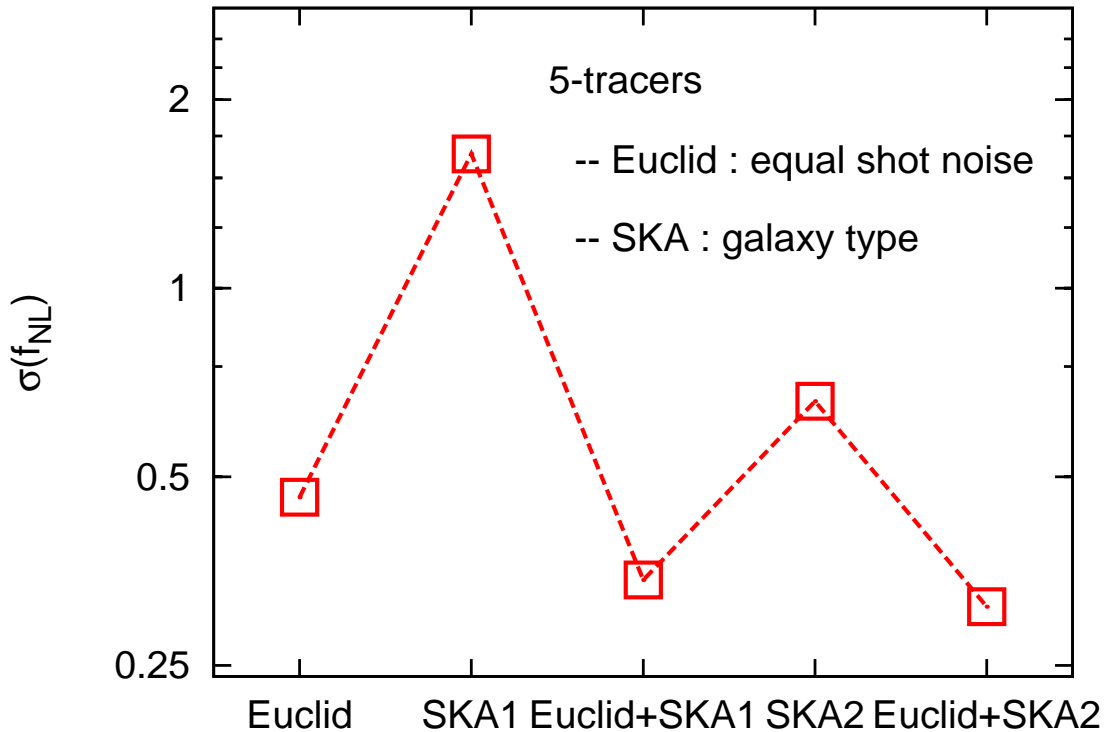


Figure 4: Expected constraints on f_{NL} from the SKA continuum survey, Euclid photometric survey and their combinations Yamauchi et al. (2014).

but if there are ongoing activities, such as merging of clusters and/or violent large-scale galactic outflows, the situation could be more complicated. Photons on different rays originating from a lensed source could therefore have different frequency dependent attenuation, through absorption and/or scattering by the matter along the rays. Moreover, if there is a spatially inhomogeneous magnetic field permeating the lens and its surrounding, polarisation fluctuations could also be induced in the lensed images. This potential frequency-dependent distortion has not been investigated in detail, however it could be inferred through multi-wavelength polarisation observations using the SKA. With the information of the matter distribution and the magnetic field along the line of sight, frequency-dependent attenuation of photons can be modelled using radiative transfer calculations and hence prescriptions for correcting the corresponding distortion and biases could be derived.

3. Systematic Synergies

The combination of power spectra discussed in the previous section will enable a mitigation systematic to be performed at the statistical level. However because Euclid and the SKA will observe many of the same galaxies one can directly compare the measurements to gain an ever larger advantage. We refer here to systematic reductions discussed in the Chapter on Weak Lensing and Synergies, and highlight here one particular aspect that is enabled through the weak lensing

shape measurement that is only possible using both Euclid and SKA, due to the PSF stability and size available from space or very wide aperture radio telescopes (see Massey et al. (2013); such observations are not possible using ground-based optical telescopes).

Optical and radio surveys, such as Euclid and SKA, have a particularly useful synergy in reducing and quantifying the impact of systematic effects which may dominate each survey alone on some scales. By cross-correlating the shear estimators from one of these surveys with those of the other, several systematic errors are mitigated. We can see this by writing the contributions to an optical (o) or radio (r) shear estimator:

$$\gamma^{(o)} = \gamma_{\text{grav}} + \gamma_{\text{int}}^{(o)} + \gamma_{\text{sys}}^{(o)} \quad (3.1)$$

$$\gamma^{(r)} = \gamma_{\text{grav}} + \gamma_{\text{int}}^{(r)} + \gamma_{\text{sys}}^{(r)} \quad (3.2)$$

$$(3.3)$$

where γ_{grav} is the gravitational shear we are seeking, γ_{int} is the intrinsic ellipticity of the object, and γ_{sys} are systematic errors induced by the telescope.

If we correlate optical shears with optical shears, or radio shears with radio shears, we obtain terms like

$$\langle \gamma\gamma \rangle = \langle \gamma_{\text{grav}} \gamma_{\text{grav}} \rangle + \langle \gamma_{\text{grav}} \gamma_{\text{int}} \rangle + \langle \gamma_{\text{int}} \gamma_{\text{int}} \rangle + \langle \gamma_{\text{sys}} \gamma_{\text{sys}} \rangle \quad (3.4)$$

where the first term is the gravitational signal we seek, the second term is the GI intrinsic alignment, the third term is the II intrinsic alignment, and the final term is the contribution from systematics. All of these terms could be similar size on certain scales, which is of damage to cosmological constraints. On the other hand, if we cross-correlate the optical shears with radio shears, we obtain

$$\langle \gamma^{(o)} \gamma^{(r)} \rangle = \langle \gamma_{\text{grav}} \gamma_{\text{grav}} \rangle + \langle \gamma_{\text{grav}} \gamma_{\text{int}}^{(o)} \rangle + \langle \gamma_{\text{grav}} \gamma_{\text{int}}^{(r)} \rangle + \langle \gamma_{\text{int}}^{(o)} \gamma_{\text{int}}^{(r)} \rangle + \langle \gamma_{\text{sys}}^{(o)} \gamma_{\text{sys}}^{(r)} \rangle \quad (3.5)$$

The second and third terms are the GI systematic alignment, which still survives. However, the fourth term involves the correlation between optical and radio shapes, which will be less than that between one frequency alone as the emission mechanisms are different (c.f. Patel et al. (2010) where no correlation at zero lag was found). This term is therefore reduced. Most importantly, the fifth term involving systematics is expected to be zero, as the systematics in these two telescopes of completely different design and function are not expected to be correlated at all. We are therefore able to remove the dangerous systematic correlations from our shear analysis - and to gain an estimate of its magnitude in the autocorrelation case.

4. Simulation Synergies

Both Euclid and the SKA will require a large number of N-body simulations in order to achieve their science objectives. These simulations will be used for a variety of purposes for example a small number of large box-size simulations can be used to generate mock catalogues that can be used in the development of data analysis algorithms by creating fake data with which to test the pipelines. In order to compute the likelihood functions used for cosmological analyses covariance matrices for data vectors will be needed. In order to characterise these realisations of data will be required (Taylor et al. 2013), and depending on the number of data points and parameters this

could result in up to $\sim 10^6$ realisations. Because the covariance matrices for cosmological observable power spectra depend on cosmology themselves this results in the potential need for tens of thousands or millions of high resolution, small box-size, simulations.

This is a significant computational task and, because at small scales the impact of baryonic feedback will be important (see for example Kitching et al. (2014)), it is likely that these simulations will need to be hydrodynamical as well as N-body. The completion of this number of simulations by 2020, in time for both Euclid and the SKA, is a challenge but because the area and depth of both surveys is synergistic it is likely that well designed simulations will meet the needs of both experiments, providing a common resource for both. Whilst common simulations will reduce the overall resources required for this task, it will also require that these simulations are potentially more sophisticated than survey-specific ones. For example a single simulation that provided a resource for both 21cm mapping and lower redshift cosmic shear may need to perform ray tracing over a substantially larger redshift range than a simulation that was tailored to either cosmological probe alone.

5. Methodological Synergies

Not only will Euclid and the SKA have many scientific synergies, but they will both provide ‘big’ (a large number of bytes) astrophysical data-sets, the analysis of which will also present many methodological synergies. In addition to the techniques already in use today to analyse optical and radio observations, recent experience from the analysis of cosmic microwave background (CMB) observations can be used to infer future methods of interest.

Bayesian statistics is the dominant paradigm for the analysis of CMB observations. Typically cosmological parameters are estimated from observational data in a Bayesian framework using Markov Chain Monte Carlo (MCMC) sampling techniques e.g. (e.g. Lewis & Bridle 2002), such as the Metropolis Hastings algorithm. If the parameter space is of moderate size, then nested sampling methods (Skilling 2004; Feroz & Hobson 2008; Feroz et al. 2009, 2013) are often used to enable the efficient calculation of the Bayesian evidence in order to distinguish between cosmological models. Such techniques are already common when analysing optical and radio observations. For high-dimensional problems, Gibbs and Hamiltonian sampling have been applied successfully to sample high-dimensional posterior distributions for CMB analysis (e.g. Wandelt et al. 2004; Taylor et al. 2008). These sampling techniques are already starting to be applied to mock galaxy surveys (Jasche et al. 2010; Jasche & Wandelt 2013a,b).

In addition to Bayesian analysis, sparsity-based approaches are gaining popularity as an alternative and complementary CMB analysis technique. First works in this area focused on the use of wavelets, which are a powerful signal analysis tool due to their ability to represent signal content in space and scale simultaneously. This property is particularly useful for the study of astrophysical signals, where the physical processes responsible for signals of interest are typically manifest on specific physical scales, while often also spatially localised. Wavelet transforms and fast algorithms defined on the sphere (e.g. Antoine & Vanderghelynst 1999; Wiaux et al. 2005; McEwen et al. 2006; Starck et al. 2006; McEwen et al. 2007a; Wiaux et al. 2008; Marinucci et al. 2008; McEwen et al. 2013; Leistedt et al. 2013) were developed for the analysis of CMB data and have proved to be particularly effective McEwen et al. 2007b. More recently, the revolutionary new paradigm of

compressive sensing has been exploited for CMB analysis. Compressive sensing (Candès et al. 2006; Donoho 2006) is a recent ground-breaking development in information theory, which goes beyond the Shannon-Nyquist sampling theorem by exploiting sparsity and which has the potential to revolutionise data acquisition in many fields (for a brief introduction see Baraniuk 2007). At its heart, compressive sensing provides a powerful framework for solving inverse problems, typically exploiting the sparse representation of signals in a wavelet dictionary. Sparse component separation techniques that exploit these ideas have been developed to recover CMB maps from observations corrupted by foreground emission (Bobin et al. 2013). There is considerable scope to extend sparsity-based approaches to the analysis of both Euclid and SKA data, leading to numerous methodological synergies.

The galaxies that will be observed by Euclid live in 3D, hence to exploit sparsity-based techniques for the analysis of Euclid data suitable 3D wavelet transforms must be constructed. Recently, wavelet transforms have been constructed specifically for the analysis of such data by Lanusse et al. (2012) and Leistedt & McEwen (2012). These constructions are complementary, where the construction of Lanusse et al. (2012) yields isotropic 3D wavelets, whereas the construction of Leistedt & McEwen (2012) yields wavelets with angular and radial aperture that can be controlled separately. Application of these wavelet transforms to galaxy surveys is underway. Specifically, such wavelet representations should be particularly useful for 3D weak lensing. For example, compressive sensing approaches have been developed already to solve the inverse problem required to recover 3D density maps from weak lensing data using hybrid 2D-1D wavelets (Leonard et al. 2012, 2014).

Sparsity-based approaches have also shown considerable promise for imaging observations from radio interferometric telescopes, such as the SKA. Compressive sensing approaches have been developed to solve the inverse problem of recovering images from the raw Fourier measurements made by interferometric telescopes, starting from idealised applications (Wiaux et al. 2009a; McEwen & Wiaux 2011), to optimising telescope configurations (Wiaux et al. 2009b), to novel imaging methodologies (Carrillo et al. 2012), to realistic imaging scenarios (Carrillo et al. 2014), and to supporting wide fields-of-view (McEwen & Wiaux 2011; Wolz et al. 2013). In addition to imaging raw data, methods to exploit sparsity have been developed to separate the 21cm emission from the epoch of reionization from foreground emission (Chapman et al. 2013).

Sparsity and compressive sensing hence show considerable potential for the analysis of both Euclid and SKA observations. Although appropriate wavelets must be constructed on the space where the data live, the application of wavelet and compressive sensing techniques to both types of observations shares many similarities. A generic approach can be taken to solve inverse problems in a compressive sensing framework across different data domains. Furthermore, the underlying convex optimisation algorithms e.g. Combettes & Pesquet (2011) developed to solve these inverse problems are largely the same and hence the same underlying codes can be used or adapted.

In summary, the analysis of the large data-sets expected from both Euclid and the SKA will exhibit many methodological synergies and will benefit considerably by the sharing of expertise, techniques, and numerical codes, both for Bayesian and sparsity-based approaches.

6. Conclusion

The concurrent development of Euclid and the SKA over the next decade, with the near simultaneous observations of significant fractions of the sky in radio wavelengths and spaced-based optical and NIR imaging and spectra represents an unprecedented era in astronomy; and step-change in data quantity and quality that is unlikely to be surpassed in the foreseeable future. The synergies between these projects is manifest, and it almost goes without saying that the combination of the science from these projects will result in more than the sum of the parts.

The synergies are many-fold enabling the experiments to mutually reduce systematic effects; improve statistical constraints on parameters, in particular for cosmology; and enable new science. In addition there are synergies on the preparatory aspects, in particular on the production of simulations, and on the exploitation of the data through methodological overlap. Specifically

- **Survey synergies.** Euclid and SKA will observe the same sky, at complementary overlapping depths, over the same time period of observation, but crucially at different wavelengths which enables independent cross-validation of results and systematics.
- **Cosmology synergies.** The combination of the two experiments can improve cosmological constraints through the simple addition of the data, but extra information from the cross-correlation is likely to allow for further gains. In particular dark energy, modified gravity and non-Gaussianity measurement may be improved significantly through the combination of Euclid and the SKA.
- **Systematic synergies.** Euclid and SKA will measure some of the same properties from the same galaxies but at different wavelengths and with different instrumental systematics. By cross-correlating it may be possible to construct estimators that have much lower (or even zero) sensitivity to particular systematics, for example those associated with galaxy weak lensing measurements.
- **Simulations & Methodological synergies.** Both Euclid and SKA will require many N-body simulations, and new methodological techniques, to support the theoretical interpretation of the observations. Given the finite resources available to the astronomy community there is an opportunity for cooperation in this area during and after the construction phases.

These synergies exist *now*, even in pre-construction, during preparation, and will continue to grow as data is accumulated. These synergies will last for decades after data is collected, involving thousands of scientists world wide in mutual collaboration.

Acknowledgments

TDK is supported by a Royal Society University Research Fellowship. MLB is supported by the an ERC Starting Grant (Grant no. 280127) and by a STFC Advanced/Halliday fellowship. RS acknowledges support from both “ASI I/023/12/0” and “MIUR PRIN 2010”. DB is supported by UK STFC grant ST/K00090X/1.

References

- Albrecht, A., Bernstein, G., Cahn, R., Freedman, W. L., Hewitt, J., Hu, W., Huth, J., Kamionkowski, M., Kolb, E. W., Knox, L., Mather, J. C., Staggs, S., & Suntzeff, N. B. 2006, ArXiv e-prints 0609591
- Amiaux, J., Scaramella, R., Mellier, Y., Altieri, B., Burigana, C., Da Silva, A., Gomez, P., Hoar, J., Laureijs, R., Maiorano, E., Magalhães Oliveira, D., Renk, F., Saavedra Criado, G., Tereno, I., Auguères, J. L., Brinchmann, J., Cropper, M., Duvet, L., Ealet, A., Franzetti, P., Garilli, B., Gondoin, P., Guzzo, L., Hoekstra, H., Holmes, R., Jahnke, K., Kitching, T., Meneghetti, M., Percival, W., & Warren, S. 2012, in Society of Photo-Optical Instrumentation Engineers (SPIE) Conference Series, Vol. 8442, Society of Photo-Optical Instrumentation Engineers (SPIE) Conference Series
- Antoine, J.-P. & Vandergheynst, P. 1999, ACHA, 7, 1
- Baraniuk, R. 2007, IEEE Sig. Proc. Mag., 24, 118
- Bobin, J., Starck, J.-L., Sureau, F., & Basak, S. 2013, A&A, 550, A73
- Camera, S., Fedeli, C., & Moscardini, L. 2014, jcap, 3, 27
- Candès, E., Romberg, J., & Tao, T. 2006, IEEE TIT, 52, 489
- Carrillo, R. E., McEwen, J. D., & Wiaux, Y. 2012, MNRAS, 426, 1223
- . 2014, MNRAS, 439, 3591
- Chapman, E., Abdalla, F. B., Bobin, J., Starck, J.-L., Harker, G., Jelić, V., Labropoulos, P., Zaroubi, S., Brentjens, M. A., de Bruyn, A. G., & Koopmans, L. V. E. 2013, MNRAS, 429, 165
- Combettes, P. & Pesquet, J.-C. 2011, Proximal splitting methods in signal processing (New York: Springer), 185–212
- Cropper, M., Cole, R., James, A., Mellier, Y., Martignac, J., Di Giorgio, A.-M., Paltani, S., Genolet, L., Fourmond, J.-J., Cara, C., Amiaux, J., Guttridge, P., Walton, D., Thomas, P., Rees, K., Pool, P., Endicott, J., Holland, A., Gow, J., Murray, N., Duvet, L., Auguères, J.-L., Laureijs, R., Gondoin, P., Kitching, T., Massey, R., & Hoekstra, H. 2012, in Society of Photo-Optical Instrumentation Engineers (SPIE) Conference Series, Vol. 8442, Society of Photo-Optical Instrumentation Engineers (SPIE) Conference Series
- Cropper, M., Hoekstra, H., Kitching, T., Massey, R., Amiaux, J., Miller, L., Mellier, Y., Rhodes, J., Rowe, B., Pires, S., Saxton, C., & Scaramella, R. 2013, MNRAS, 431, 3103
- Donoho, D. 2006, IEEE TIT, 52, 1289
- Fedeli, C. & Moscardini, L. 2012, jcap, 11, 55
- Feroz, F. & Hobson, M. P. 2008, MNRAS, 384, 449

- Feroz, F., Hobson, M. P., & Bridges, M. 2009, MNRAS, 398, 1601
- Feroz, F., Hobson, M. P., Cameron, E., & Pettitt, A. N. 2013, ArXiv e-prints 1306.2144
- Heavens, A., Alsing, J., & Jaffe, A. H. 2013, MNRAS, 433, L6
- Jasche, J., Kitaura, F. S., Wandelt, B. D., & Enßlin, T. A. 2010, MNRAS, 406, 60
- Jasche, J. & Wandelt, B. D. 2013a, MNRAS, 432, 894
- . 2013b, ApJ, 779, 15
- Jimenez, R., Kitching, T., Peña-Garay, C., & Verde, L. 2010, jcap, 5, 35
- Joachimi, B., Mandelbaum, R., Abdalla, F. B., & Bridle, S. L. 2011, aap, 527, A26
- Kitching, T. D., Heavens, A. F., Alsing, J., Erben, T., Heymans, C., Hildebrandt, H., Hoekstra, H., Jaffe, A., Kiessling, A., Mellier, Y., Miller, L., van Waerbeke, L., Benjamin, J., Coupon, J., Fu, L., Hudson, M. J., Kilbinger, M., Kuijken, K., Rowe, B. T. P., Schrabback, T., Semboloni, E., & Velander, M. 2014, MNRAS, 442, 1326
- Lanusse, F., Rassat, A., & Starck, J.-L. 2012, A&A, 540, A92
- Laureijs, R. 2009, ArXiv e-prints 0912.0914
- Laureijs, R., Amiaux, J., Arduini, S., Auguères, J. ., Brinchmann, J., Cole, R., Cropper, M., Dabin, C., Duvet, L., Ealet, A., & et al. 2011, ArXiv e-prints 1110.3193
- Leistedt, B. & McEwen, J. D. 2012, IEEE TSP, 60, 6257
- Leistedt, B., McEwen, J. D., Vanderghenst, P., & Wiaux, Y. 2013, A&A, 558, 1
- Leonard, A., Dupé, F.-X., & Starck, J.-L. 2012, A&A, 539, A85
- Leonard, A., Lanusse, F., & Starck, J.-L. 2014, MNRAS
- Lewis, A. & Bridle, S. 2002, PRD, 66, 103511
- Marinucci, D., Pietrobon, D., Balbi, A., Baldi, P., Cabella, P., Kerkyacharian, G., Natoli, P., Picard, D., & Vittorio, N. 2008, MNRAS, 383, 539
- Massey, R., Hoekstra, H., Kitching, T., Rhodes, J., Cropper, M., Amiaux, J., Harvey, D., Mellier, Y., Meneghetti, M., Miller, L., Paulin-Henriksson, S., Pires, S., Scaramella, R., & Schrabback, T. 2013, MNRAS, 429, 661
- McEwen, J. D., Hobson, M. P., & Lasenby, A. N. 2006, ArXiv e-prints 0609159
- McEwen, J. D., Hobson, M. P., Mortlock, D. J., & Lasenby, A. N. 2007a, IEEE TSP, 55, 520
- McEwen, J. D., Vanderghenst, P., & Wiaux, Y. 2013, in SPIE Wavelets and Sparsity XV

- McEwen, J. D., Vielva, P., Wiaux, Y., Barreiro, R. B., Cayón, L., Hobson, M. P., Lasenby, A. N., Martínez-González, E., & Sanz, J. L. 2007b, *JFAA*, 13, 495
- McEwen, J. D. & Wiaux, Y. 2011, *MNRAS*, 413, 1318
- Patel, P., Bacon, D. J., Beswick, R. J., Muxlow, T. W. B., & Hoyle, B. 2010, *MNRAS*, 401, 2572
- Seljak, U. 2009, *Physical Review Letters*, 102, 021302
- Skilling, J. 2004, in *American Institute of Physics Conference Series*, Vol. 735, American Institute of Physics Conference Series, ed. R. Fischer, R. Preuss, & U. V. Toussaint, 395–405
- Starck, J.-L., Moudden, Y., Abrial, P., & Nguyen, M. 2006, *A&A*, 446, 1191
- Taylor, A., Joachimi, B., & Kitching, T. 2013, *MNRAS*, 432, 1928
- Taylor, J. F., Ashdown, M. A. J., & Hobson, M. P. 2008, *MNRAS*, 389, 1284
- Wandelt, B. D., Larson, D. L., & Lakshminarayanan, A. 2004, *PRD*, 70, 083511
- Wiaux, Y., Jacques, L., Puy, G., Scaife, A. M. M., & Vandergheynst, P. 2009a, *MNRAS*, 395, 1733
- Wiaux, Y., Jacques, L., & Vandergheynst, P. 2005, *ApJ*, 632, 15
- Wiaux, Y., McEwen, J. D., Vandergheynst, P., & Blanc, O. 2008, *MNRAS*, 388, 770
- Wiaux, Y., Puy, G., Boursier, Y., & Vandergheynst, P. 2009b, *MNRAS*, 400, 1029
- Wilman, R. J., Miller, L., Jarvis, M. J., Mauch, T., Levrier, F., Abdalla, F. B., Rawlings, S., Klöckner, H.-R., Obreschkow, D., Olteanu, D., & Young, S. 2008, *MNRAS*, 388, 1335
- Wolz, L., McEwen, J. D., Abdalla, F. B., Carrillo, R. E., & Wiaux, Y. 2013, *MNRAS*, 436, 1993
- Yamauchi, D., Takahashi, K., & Oguri, M. 2014, *ArXiv e-prints* 1407.5453